Cellular Response to Heat Shock Studied by Multiconfocal Fluorescence Correlation Spectroscopy

Meike Kloster-Landsberg,[†] Gaëtan Herbomel,[‡] Irène Wang,[†] Jacques Derouard,[†] Claire Vourc'h,[‡] Yves Usson,[§] Catherine Souchier,[‡] and Antoine Delon[†]*
[†]University of Grenoble I/Centre National de la Recherche Scientifique, Laboratoire Interdisciplinaire de Physique, Grenoble, France;
[‡]University of Grenoble I/Institut National de la Santé et de la Recherche Médicale, Institut Albert Bonniot, U823 team 10, Grenoble, France;
and [§]University of Grenoble I/Centre National de la Recherche Scientifique, Laboratoire TIMC-IMAG, Grenoble, France

ABSTRACT Heat shock triggers a transient and ubiquitous response, the function of which is to protect cells against stress-induced damage. The heat-shock response is controlled by a key transcription factor known as heat shock factor 1 (HSF1). We have developed a multiconfocal fluorescence correlation spectroscopy setup to measure the dynamics of HSF1 during the course of the heat-shock response. The system combines a spatial light modulator, to address several points of interest, and an electron-multiplying charge-coupled camera for fast multiconfocal recording of the photon streams. Autocorrelation curves with a temporal resolution of 14 μs were analyzed before and after heat shock on eGFP and HSF1-eGFP-expressing cells. Evaluation of the dynamic parameters of a diffusion-and-binding model showed a slower HSF1 diffusion after heat shock. It is also observed that the dissociation rate decreases after heat shock, whereas the association rate is not affected. In addition, thanks to the multiconfocal fluorescence correlation spectroscopy system, up to five spots could be simultaneously located in each cell nucleus. This made it possible to quantify the intracellular variability of the diffusion constant of HSF1, which is higher than that of inert eGFP molecules and increases after heat shock. This finding is consistent with the fact that heat-shock response is associated with an increase of HSF1 interactions with DNA and cannot be explained even partially by heat-induced modifications of nuclear organization.

INTRODUCTION

The cellular environment is a highly heterogeneous and crowded medium that exhibits fast spatial and temporal changes. For this reason, it is important to develop fluorescence fluctuation microscopy (FFM) methods that enable simultaneous measurements of dynamics at different locations within a living cell. Not only would such methods provide more complete information about the cellular machinery, but by making it possible to perform a large number of measurements in parallel, they would yield statistically significant results and assess cellular variability in a more time-efficient way.

Among the recent developments in FFM, three branches of spectroscopy can be distinguished: temporal image correlation spectroscopy, and especially raster image correlation spectroscopy, which exploits the information implicitly embedded in confocal images recorded under various modalities; scanning fluorescence correlation spectroscopy (sFCS), where autocorrelation function (ACF) curves are constructed with repeated scans of the same 1D zone (usually linear or circular); and multipoint or multiconfocal FCS (mFCS) techniques, which utilize multiple laser spots.

A more recent development of image correlation spectroscopy (1–3), raster image correlation spectroscopy is a modality that makes it possible to measure correlation between pixels, lines, and frames, to provide dynamic information at various temporal and spatial scales (4–7). However, this modality requires a rather large region of interest (ROI) to extract correlation functions of good quality. It is possible, instead of using a laser scanning microscope, to acquire a wide-field image with a fast and sensitive camera (e.g., an electron-multiplying charge-coupled device (EMCCD)), provided optical sectioning is completed in situ. One method that could be used for this is total internal reflection fluorescence microscopy (8); a second is light-sheet illumination (9). A general drawback to these two later methods, which is a direct consequence of CCD technology, is that the larger the field of view, the slower is the temporal resolution.

It might appear smarter, when acquiring FCS images, to scan only the ROI but along a chosen laser trajectory (10,11). This technique, called sFCS, has been applied with various modalities (12–17). However, here also there is a compromise between temporal resolution, spatial resolution, and spatial extension. Since only one laser spot is used at a time, one cannot get independent measurements at different points arbitrarily located within the ROI with the temporal resolution of single-point FCS.

To solve this technical drawback, it is necessary to develop optical systems that provide separated laser spots with flexible locations in the field of view. Such possibilities are offered by the dual-head confocal microscope approach, which makes it possible either to place two laser spots anywhere in the field of view, with the ultimate temporal resolution of a standard FCS microscope, or to perform

---

sFCS (18). Another tool, the spinning-disk confocal microscope, represents a promising way to flexibly address numerous laser spots (up to ~10^4) within the ROI (19,20), but one often encounters limitations with this system in terms of temporal resolution. There is nevertheless one multiple-spot technique, time-integrated multipoint moment analysis, that is capable of probing fast timescales (down to 20 μs) at hundreds of different locations in the sample simultaneously (21). A benefit of this technique is the possibility of varying the exposure times from long to very short values, even using the full area of the CCD chip. Although quite promising, this approach is, technically speaking, rather hard to implement and needs to be made more user-friendly.

We believe that there is still a need for a multiconfocal FCS system for living cell studies that would include 1), a flexible way to simultaneously address the desired laser spots at various locations within the biological specimen; and 2), a matrix of fast, pointlike detectors.

Concerning the excitation path, spatial light modulators (SLMs) are now used for microscopy applications, mainly for optical tweezers (22) and adaptive optics, to control the laser illumination geometry. We recently demonstrated the potential of SLMs for mFCS by measuring, at the single-particle level, both active transport (i.e., a flow) and passive transport (in the latter case, permeability through a phospholipidic membrane) (23). Concerning the detection path, EMCCD cameras are especially promising, since each pixel is a single-photon pointlike detector (24–26), while the on-chip amplification makes it compatible with a fast readout rate (10 MHz) and a high signal/noise ratio. It is nevertheless worthwhile to mention complementary-metal-oxide-semiconductor-single–photon-avalanche-diode (CMOS-SPAD) cameras, which combine the sensitivity of EMCCD and the frame rate of CMOS architecture (27).

Later, we report recent results obtained with an mFCS system built by combining an SLM, to address several points of interest, with an EMCCD camera for fast multiconfocal recording of the corresponding photon streams with a time resolution of 14 μs. Compared to our previously published proof of concept (28), this article presents an experimental setup by which time resolution is improved by a factor of 7, thanks to a special readout mode of a single row. Progress has also been made in acquisition speed, epifluorescence illumination, user interface, and spot positioning, so that the experiment is now truly suitable for biological studies in living cells.

This device was used to analyze the dynamics of the heat-shock factor 1 (HSF1) in living cells. The heat-shock response is characterized by two contrasting phenomena, the activation of heat shock (hsp) genes on one hand and the global repression of most cellular genes on the other. Both events correlate with important structural modification of chromatin organization and structure (29). HSF1 is the key transcription factor of the heat-shock response

(30,31), controlling heat-induced genome-wide chromatin remodeling events. Upon heat shock, HSF1 is rapidly converted into an active form, trimerizes, and acquires its capacity for DNA-binding to heat-shock elements (HSEs) present within hsp gene promoters. The way HSF1 represses global gene expression is still unclear but seems to involve its DNA-binding capacity and/or its transient interactions with repressive complexes (29). In this context, we sought to determine the dynamics of HSF1 to evaluate the DNA-binding capacity of HSF1 in unstressed and stressed living cells. Moreover, since heat shock is known to induce major modifications of nuclear structure, data obtained on HSF1 were compared to data obtained on enhanced green fluorescent protein (eGFP) molecules with no DNA-binding competency, to distinguish structure-related changes from interaction changes. Diffusion and DNA binding of transcription factors are coupled processes that occur on extended timescales from tens of microseconds to tens of minutes. The simplest representation of this complex mechanism assumes a pool of free-diffusing molecules interacting with fixed binding sites. The question therefore arises as to which factors (diffusion, association, or dissociation rates) are affected by the heat-shock response. Further, are these quantities homogeneously distributed within the nucleus, thus meaning that they are dominated by numerous relatively nonspecific interactions, or, conversely are they rather inhomogeneous because of a limited number of more specific binding sites? Also, are these distributions modified during heat-shock response?

Using the mFCS system, heat shock was induced under the microscope and parallel acquisitions were performed in five nuclear spots, allowing analysis of intranuclear variability in a short enough time and, consequently, a reliable study of the spatial distribution of the dynamics. Compared to single-point FCS, our method not only reduces significantly the total acquisition time, but avoids any entanglement between spatial and temporal variations.

In the next section, we describe the experimental device. To characterize the system, mFCS measurements were performed with fluorescent dye solutions, as reported in the Results section. Finally, the results obtained on the dynamics of eGFP and HSF1-eGFP in living cells are presented.

MATERIAL AND METHODS

Dye solutions

FCS and mFCS measurements in solution were performed using Rhodamine 6G (Radiant Dyes, Wermelskirchen, Germany) and Dextran-Rhodamine Green 10 kDa (Life Technologies, Grand Island, NY). To avoid aggregation, Dextran-Rhodamine Green molecules were prepared in buffer solution at pH 8.2. These molecules were used without further purification and diluted at concentrations of a few tens of nM to 1100 nM. Purified recombinant eGFP protein was also used (Clontech, Mountain View, CA).

Cell culture

Human brain glioblastoma U87 cells were cultured in Dulbecco's modified Eagle's medium (DMEM; PAA, Pashing, Austria) supplemented with 10% fetal calf serum, 2% glutamine (4 mM), and 1% nonessential amino acids in 5% CO_2 atmosphere at 37°C. Cells were transfected with reporter plasmids expressing the human HSF1-eGFP with Lipofectamine 2000 transfection reagent (Life Technologies). Stable HSF1-eGFP cell lines were established using geneticin and a flow-cell sorting system (FACSAria, Beckton Dickinson, San Jose, CA) for selecting transfected cells expressing a low level of HSF1-eGFP adapted for FCS. A stable Hela cell line expressing only the eGFP protein was also used. Two days before the experiments, cells were plated on culture dishes (Bioptechs, Butler, PA). Data acquisition under the microscope was performed in DMEM medium without phenol red supplemented with 1% fetal calf serum, 2% glutamine, and 10 mM Hepes. Heat shock was performed at 43°C for 1 h using a temperature-control system that involved stage and objective control (Delta T, Bioptechs).

Multiconfocal FCS setup and data acquisition

The FCS measurements were performed on an improved version of a homebuilt setup (28) (Fig. S1 in the Supporting Material). An SLM is used to split the laser beam and create several excitation spots at freely chosen locations in the focal plane of the objective lens (Plan-Apo 60×, NA 1.2, Olympus, Rungis, France). Fluorescence can be detected by either an avalanche photodiode (APD) for single-spot FCS measurements or an EMCCD (iXon+ DU860, Andor Technology, Belfast, Ireland) for parallel multispot measurements.

The phase map applied to the SLM is calculated using a spherical wave and superposition approach, as previously described (28,32). The principle of the algorithm is simple: we assume that each desired spot results from a converging spherical wave. Then the phase function is obtained from the back-propagation and superposition of the spherical wavefronts in the plane of the SLM. The corresponding details and Eq. S2 are presented in the Supporting Material.

For single-spot FCS, the APD signal is processed by a homemade electronic counter and recorded using a data acquisition board and software correlated by a program developed in Delphi (Borland, Austin, TX), to provide the ACF. We also calculate the molecular brightness, defined as the ratio of the count rate (in kHz) to the number of molecules, as obtained by fitting the ACF curve.

For mFCS, a software environment developed in Matlab (MathWorks, Natick, MA) controls the experiment and performs data acquisition and processing. The EMCCD camera was used in the Crop FvB (full vertical binning) readout mode, with all the spots aligned on the bottom row of the chip, so that a 70 kHz frame rate could be achieved, resulting in a 14 μs time resolution. More details on data acquisition and processing are given in the Supporting Material.

ACF fit model

Among the numerous models of ACFs that can be found in the literature, the choice of the best model to represent the dynamics of the detected molecules is a key issue. For the biological situation presented here, we believe that the best choice is the model called reaction-dominant, derived by Michelman-Ribeiro et al. (33). It stems from a general situation of equilibrium, where molecules with diffusion constant D can reversibly bind to an immobile substrate with a pseudoassociation rate, $k_{on}*$ (which incorporates the equilibrium concentration of vacant binding sites), and a dissociation rate, k_{off}. In the simplified reaction-dominant regime, the diffusion time across the confocal volume, $\tau_D = w_r^2/4D$, is much shorter than the average time to associate with a binding site, i.e., $\tau_D << 1/k_{on}*$. As a consequence, the ACF, $G(\tau)$, can be decomposed to yield

$$G(\tau) = 1 + \frac{1}{N}\left[F_{eq}\left(1 + \frac{\tau}{\tau_D}\right)^{-1}\left(1 + \frac{\tau}{(S^2\tau_D)}\right)^{-1/2} \right.$$
$$\left. + C_{eq}e^{-\tau/\tau_{off}} \right], \tag{1}$$

where N is the effective number of molecules in the FCS effective volume, S is the usual structure parameter (ratio of the longitudinal to the transverse radii of the confocal volume, $S = w_z/w_r$), $\tau_{off} = k_{off}^{-1}$, and

$$F_{eq} = 1 - C_{eq} = \frac{k_{off}}{k_{off} + k_{on}^*} \tag{2}$$

is the free fraction of molecules. Note that we did not include any triplet term in the ACF, because the temporal resolution of our setup (14 μs) does not reach to the characteristic time of triplet relaxation (34). Due to the appearance of a superimposed oscillation at very long lag times (~1 s), we had to include in the model an additional temporal component to properly describe our experimental results. We could not unambiguously identify the physical origin of this artifact, but since it manifests as an oscillation superimposed on the ACF curves, we assumed that the detected signal, $s(t)$, was amplitude-modulated with a period T and a relative modulation depth of a, that is,

$$s(t) = f(t)\left[1 + a \times \cos\left(\frac{2\pi t}{T} + \varphi\right)\right], \tag{3}$$

where $f(t)$ is the fluorescence signal that would be detected if there were no artifact, and its ACF of which is given by Eq. 1. Consequently, the ACF of the detected signal is

$$G_s(\tau) = G(\tau)\left[1 + \frac{a^2}{2}\cos\left(\frac{2\pi\tau}{T}\right)\right]. \tag{4}$$

Note that the phase, φ, does not appear in the ACF. Altogether, the adjusted parameters are a, N, F_{eq}, τ_D, and τ_{off} (practically, T was fixed at 1.8 s and S at 5).

Because T and τ_{off} have close orders of magnitude, we statistically checked the fits and observed that there was no correlation between the oscillation parameter a and the residence time τ_{off}, thus validating the meaning of the latter parameter.

Performances of EMCCD versus APD detection for FCS

The performance of the EMCCD camera as a detector for FCS was compared to the standard APD over a wide range of fluorophore concentrations and laser powers. In Fig. S4, we show that the performance of the EMCCD comes close to that of the APD. More detailed information can be found in the Supporting Material.

RESULTS AND DISCUSSION

Measurements in solution

FCS calibration with single and multiple excitation spots

To characterize our multiconfocal FCS setup under controlled conditions, measurements in solution were performed. All calibration measurements and corresponding data are presented in the Supporting Material. Only a synthetic summary is given below.

Single-spot measurements were performed to calibrate the FCS observation volume. Dextran-Rhodamine Green 10 kDa in water was chosen as a reference sample, since its large size and thereby slow diffusion is compatible with the time resolution of the EMCCD camera (14 μs). By comparing its residence time with that of Rhodamine 6G (using APD detection), we deduced the diffusion coefficient of Dextran-Rhodamine Green 10 kDa at 37°C: $D_{Dext} = 161 \ \mu m^2/s$. Then, solutions of various concentrations were measured with both the APD and the EMCCD detector pathways. The observation volume was found to increase by ~30% for EMCCD detection relative to APD detection. We estimate the lateral dimension of the observation volume (assumed to be a 3D Gaussian) at $w_r = 0.251 \ \mu m$ for the overall setup, which combines the SLM (to generate a single spot) and the EMCCD. When the excitation spot is moved away from the optical axis, no significant enlargement of the observation volume is detected within a 10 μm radius from the center. All the excitation spots used in this work are within this range.

When several excitation spots are simultaneously generated by the SLM, we do not observe any change in the width of the effective volume compared to the single-spot case. However, spurious values of the estimated number of molecules are obtained due to signal cross talk between adjacent spots. The signal detected for each spot is obscured by contributions from adjacent spots that create an unwanted background and result in an artificial increase in the estimated number of molecules. We corrected this effect by quantifying the contribution of different spots using a multipeak Lorentzian fit of the average fluorescence profile and subtracting the resulting background from the time trace before calculating the ACF. More details about calibration in solution and cross-talk correction are given in the Supporting Material (see in particular Fig. S5 for single-spot measurements and Fig. S6 for multiple spots).

For all single-spot measurements in solution, the laser power at the exit of the single-mode fiber was set to 80 μW. For multispot measurements (five spots), the total laser power was set to 500 μW (that corresponds to ~80 μW/spot, taking into account the nondiffracted light). The spots were never located according to any pattern, to avoid additional phantom spots.

Besides characterization purposes, measurements in solution are routinely performed to check the optical alignment: before each experiment on cells, a Dextran-Rhodamine Green solution is measured with the same spot series as in the forthcoming cell acquisitions.

Diffusion of eGFP in aqueous solution

For a comparison with eGFP behavior in living cells, which will be the subject of a subsequent study, we determined the diffusion coefficient and brightness of eGFP in solution at various temperatures ranging from 25°C to 43°C to investigate the temperature-dependent changes that may affect our measurements in cells. We used a single SLM-generated spot and the APD as detector. The ACF curves were fitted with a one-component diffusion model. The resulting diffusion time varied from 94 μs at 25°C to 63 μs at 43°C. Using the previously determined width of the observation volume ($w_r = 0.211 \ \mu m$), we can deduce the following range of diffusion coefficients: $D_{25°C} = 119 \ \mu m^2/s$ to $D_{43°C} = 177 \ \mu m^2/s$ (with $D_{37°C} = 155 \ \mu m^2/s$). Fig. S7 shows the diffusion coefficient variation over the entire temperature range, together with the expected variation calculated from the change in water viscosity. A good correlation is found, indicating an absence of eGFP conformational changes in this temperature range. The resulting diffusion coefficient is in reasonable agreement with previously published values: it is 14% higher than the value obtained by sFCS (35) when the temperature correction is applied. Concerning eGFP brightness, although we observed a distinct reduction in brightness when the temperature increases from 25°C to 43°C, only a slight decrease (~11%) occurs between 37°C and 43°C.

eGFP experiments in living cells

Measurement protocol with living cells

Hela cells stably expressing eGFP were used to control our experimental mFCS protocol in living cells. This protocol consists of performing mFCS measurements on five cells per culture dish, with typically three dishes observed during one day of experiments. The laser power at the exit of the single-mode fiber was limited to 120 μW, a compromise between photobleaching and signal/noise ratio of the ACF curves. Before starting a series of acquisitions on a culture dish, five laser spots were created with the SLM and were automatically aligned on the pixels of the EMCCD camera. These spots are irregularly distributed along a line at a mean distance of 3~4 μm. A sample of Dextran-Rhodamine Green was systematically used before and after each culture-dish measurement (which took ~2 h) to verify the middle-term stability of the set-up. Five cells were consecutively selected and measured at 37°C, with the nucleus in focus, then heat-shocked for 1 h to be imaged and measured again at 43°C. We always performed two measurements per cell, which consist of recording five 10 s acquisitions (plus an acquisition without laser for offset correction; see Supporting Material) and averaging their ACFs. Between the two measurements, the positions of the five spots are shifted within the cell. To verify that our results were not biased by the slight variability of the laser-spot intensities and focusing, we looked for correlations between the diffusion times of the spots in the reference Dextran-Rhodamine Green solution and those measured afterward in the cells. We never found such correlation, indicating that systematic differences between spots are negligible and that the intracellular variability

of the estimated parameters is much higher than their instrumental noise.

Altogether, the Hela-eGFP campaign of measurements provided 150 averaged ACF curves for each temperature, among which 10 curves were rejected, because the corresponding laser spots were not properly located in the cell and gave unusable ACFs. The majority of the spots were located in the nucleus, with only a few in the nucleoli and the remaining ones located mostly in the cytoplasm. The 280 retained ACF curves could be properly fitted with the standard 3D free-diffusion model (which corresponds to Eq. 1 by setting $F_{eq} = 1$).

Only the brightness of the inert eGFP molecules is affected by heat shock

Fig. 1 *A* shows the ACF curves of four spots located within the nucleus of a given cell at 37°C, the fifth one being in the cytoplasm. We see in Fig. 1 *B* a comparison between ACFs averaged over five nuclei at 37°C and 43°C, which illustrates the weak difference in dynamics and concentration between the two temperatures. To go further, we performed analysis of variance (ANOVA) of the diffusion time, τ_D, and the number of molecules, N, to test which factors were significant. Moreover, to check that the heat shock does not induce any irreversible experimental artifact, one of the three Hela-eGFP culture dishes was first heated and measured at 43°C, then cooled down and measured at 37°C, whereas the two other dishes were measured in

FIGURE 1   ACFs obtained with eGFP cells. (*A*) Example of ACF curves acquired from four spots located in the nucleus (spots 1–4) and one in the cytoplasm (spot 5) of a single eGFP cell at 37°C. (*Inset*) Locations of the spots, marked by crosses, on a wide-field fluorescence image of the cell. (*B*) Averaged ACF curves corresponding to 38 spots at 37°C (*blue circles*) and 38 spots at 43°C (*red triangles*) located in the nuclei of five eGFP cells. Superimposed black solid lines correspond to the fits. (*Inset*) Estimated parameters.

normal sequence (first at 37°C, then at 43°C). In conclusion, the temperature, measurement sequence, and localization within the cells are not significant factors with regard to τ_D and N. Conversely, we observed that the global intensity decreases by 23% at the higher temperature. Since temperature has no significant effect on the number of molecules, this corresponds to a decrease of the molecular brightness by 23% (going from 37° to 43°C), which is reasonably consistent with our measurements of eGFP in solution. Globally the diffusion time varies between 314 and 588 μs (first and last quartiles, respectively), with a median at 422 μs. Using the radius of the observation volume ($w_r = 0.251 \ \mu m$), we also calculated the median value of the diffusion-constant distribution and found it to be 37 $\mu m^2/s$, that is, about four times lower than the value measured in solution. Moreover, the distribution of its value is rather broad, in fairly good agreement with Oh et al. (21) and Dross et al. (36).

The reaction-dominant model is not necessary to fit the eGFP data

In addition, to treat on an equal footing the dynamics of HSF1-eGFP cells and that of eGFP cells, we also fitted the ACF curves of the eGFP cells with the complete reaction-dominant model by leaving free the parameters F_{eq} and τ_{off} (see Eq. 1). Although the corresponding reduced χ^2 statistics does not indicate better fits, this allows further discussion about HSF1 dynamics and comparisons with eGFP cells. In agreement with the pure diffusion fits, the temperature has no influence on the parameters of the reaction-dominant fits (τ_D, F_{eq}, and τ_{off}). However, the median diffusion constant now increases to 79 $\mu m^2/s$, because part of the long-time behavior of the ACF is taken into account by the parameter τ_{off}. Interestingly enough, among the initial set of 280 ACF curves, ~30% of the fits could not properly converge or led to aberrant parameter values, meaning that in those situations, the F_{eq} and τ_{off} parameters were ill-defined (whereas the pure diffusion model held). In contrast, for HSF1-eGFP cells, >93% of the ACF curves could be properly fitted using the reaction-dominant model, as discussed below (conversely, they could not be fitted with the free-diffusion model).

Cellular response to heat shock

We applied to HSF1-eGFP-expressing cells the same protocol used for eGFP-expressing control cells, except that the fits were all performed with the reaction-dominant model, since the pure-diffusion model gave a bad quality of fit. Experiments were performed on 12 culture dishes and provided 330 correct fits of the ACF curves at 37°C and 344 at 43°C, all corresponding to spots located in the nuclei (excluding nucleoli), where HSF1-eGFP concentrates. Rejected incorrect fits (7%) correspond to estimated parameters that were either inconsistent with the model
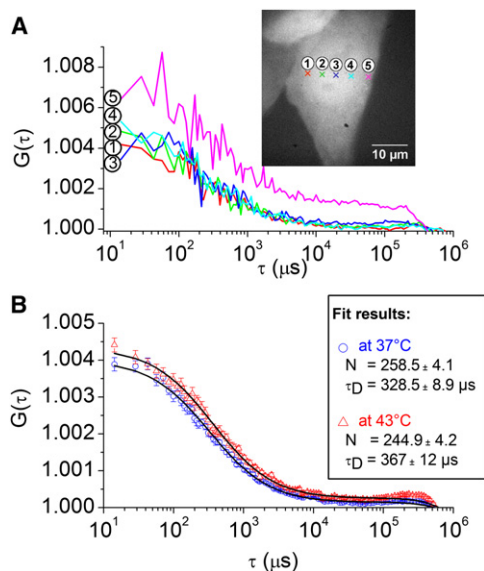
(34), or farther by a factor of 10 from the mean value. After heat shock, HSF1-eGFP is partially relocalized within nuclear stress bodies (nSBs). The presence of these nSBs was used as a control of efficient heat-shock cellular response, but all the measurements were performed outside nSBs (otherwise, a strong photobleaching is induced, which makes mFCS data nonexploitable). In contrast to the case for eGFP-expressing cells, a clear impact of heat shock was observed on HSF1-eGFP-expressing cells, as discussed in the next section.

Number of molecules decreases after heat shock

As shown in Fig. 2, A and B, at 43°C the number of molecules is significantly lower, whereas the dynamics is slower. A statistical analysis of the whole set of HSF1-eGFP data shows that the intensity and the number of molecules both decrease by a factor of 2 when going from 37°C to 43°C. In other words, the molecular brightness does not significantly change, which differs from the case for eGFP cells. The pronounced decrease in intensity can be attributed to two factors: HSF1 relocalization within the nSBs and the consequence of DNA binding of HSF1-eGFP molecules favoring photobleaching. Moreover, we suggest that the brightness is maintained between 37°C and 43°C (in contrast to eGFP cells) because of the interplay between trimerization of HSF1, photobleaching, and decrease of eGFP
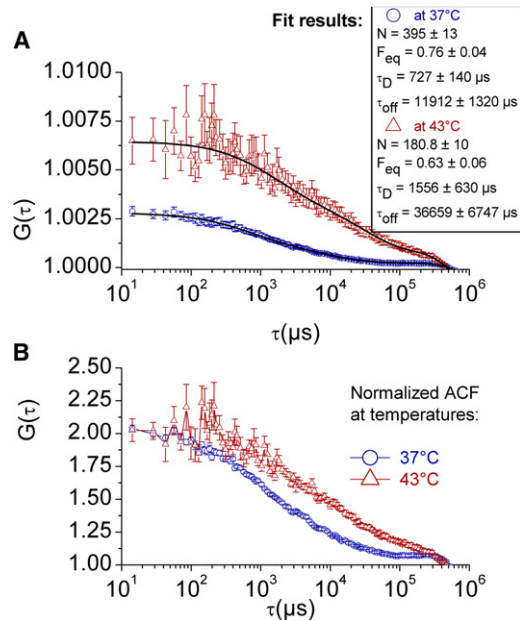
molecular brightness. Thus, three phenomena contribute to the decrease in the number of molecules: photobleaching, nSB relocalization, and trimerization.

Photobleaching shows very-long-time dynamics

To get a better overview of relocalization and photobleaching, we plotted in Fig. 3 the relative intensities during the time course of acquisitions (two series of five acquisitions at each temperature) and also compared HSF1-eGFP cells to eGFP cells. First, we observe for HSF1-eGFP cells only a sharp drop in intensity between the last acquisition at 37°C and the first one at 43°C. This is clearly the consequence of nSB relocalization. Such a pronounced drop in intensity is not observed with eGFP cells, where the limited drop can be attributed solely to the decrease in brightness. At each temperature, we also observe at the beginning of the second series of five acquisitions (new spot location) a partial reinitialization of the fluorescence intensity of HSF1-eGFP cells. This can be due to weakly mobile species: when the spots are shifted to the second series of positions, fresh, weakly mobile species start being photobleached. Such weakly mobile species do not exist in eGFP cells, where the decrease in intensity at each temperature is monotonous. The weakly mobile HSF1-eGFP species must have a residence time of the order of 1 s or longer, i.e., a time inaccessible to mFCS, which is limited to times $<\sim1$ s. Another explanation could be compartmentalization, which would induce a local depletion in the vicinity of the spots.

Diffusion and dissociation rate slow down after heat shock

As can be seen in Fig. 4, A–C, the fit parameters τ_D, τ_{off}, and F_{eq} are strongly affected by heat shock and between 37°C and 43°C vary from 956 to 2788 μs, from 31970 to 48640 μs, and from 0.71 to 0.55 (mean values), respectively. We checked that the uncertainties of the individual fit

FIGURE 2 Averaged ACF curves corresponding to 32 spots at 37°C (*blue circles*) and 13 spots at 43°C (*red triangles*) located in the nuclei of five HSF1-eGFP cells. (*A*) Fits without any prior normalization of the individual curves, to reveal the difference of amplitude due to the change in the number of molecules. Superimposed black solid lines correspond to the fits. (*Inset*) Estimated parameters. (*B*) Fits with normalization of the amplitude ($G(0) = 2$) of each individual ACF curve, to emphasize the difference in temporal behavior.
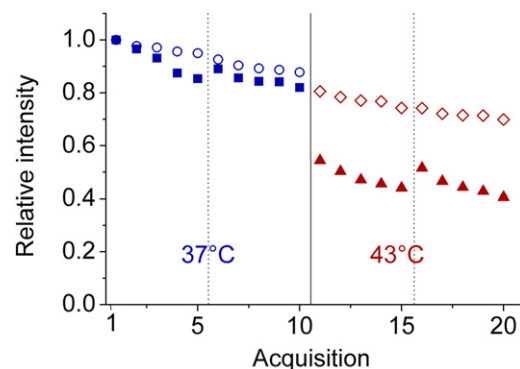

FIGURE 3 Relative variation of intensities during the time course of acquisitions before and after heat shock. The successive series of five acquisitions are separated by dotted vertical lines, whereas data for the two temperatures are separated by a solid line. Open symbols correspond to eGFP cells (*blue circles*, 37°C; *red diamonds*, 43°C) and solid symbols to HSF1-eGFP cells (*blue squares*, 37°C; *red triangles*, 43°C).
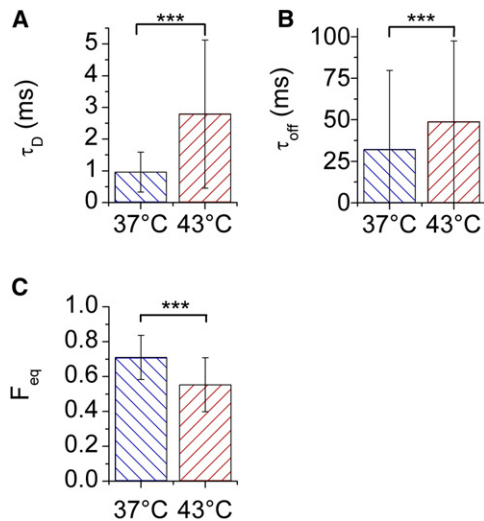
FIGURE 4 Mean values and SDs (*vertical bars*) of the diffusion time, τ_D (*A*), residence time, τ_{off} (*B*), and fraction of free molecules, F_{eq} (*C*), before (*left*) and after heat shock (*right*), obtained by fitting 330 ACF curves at 37°C and 344 ACF curves at 43°C. The symbol *** corresponds to a significance level $P < 10^{-3}$ between the bracketed groups.

parameters are smaller than the SDs of their global distributions, thus meaning that these distributions reflect some cellular variability. To proceed further, we first consider the median values of three dynamic constants, D, $k_{on}*$, and k_{off}, calculated from their distributions shown in Fig. S8.

The diffusion constant of HSF1-eGFP is 18 μm^2/s at 37°C and 7.2 μm^2/s at 43°C. From these values we can estimate the molecular mass of HSF1-eGFP, which would be 286 kDa at 37°C and 4470 kDa at 43°C. Although the value for non-heat-shocked cells is consistent with gel filtration data (220–330 kDa), the molecular mass for heat-shocked cells is significantly larger than that obtained by gel filtration (700–800 kDa) (37,38). In other words, our measured D constant is too small at 43°C. We thus suggest that the diffusion constant measured after heat shock is an effective diffusion constant slowed down by various interactions. Only the less specific of these interactions is directly measured by mFCS, corresponding to rather fast association and dissociation events.

The k_{on} and k_{off} constants are found to be $k_{on}* = 22.4$ s^{-1} and $k_{off} = 65$ s^{-1} at 37°C versus $k_{on}* = 23.2$ s^{-1} and $k_{off} = 30.1$ s^{-1} at 43°C. A surprising finding was that although k_{off} is affected by heat shock, $k_{on}*$ is not. As suggested previously, we cannot directly evaluate the more specific part of the $k_{on}*$ distribution after heat shock. Since the measured value of $k_{on}*$ is related to less specific interactions, it does not change after heat shock. For eGFP cells, a higher value of $k_{on}* = 47.4$ s^{-1} was found. Since the diffusion of those cells is also twice as fast as that of HSF1 cells before heat shock, we believe the measured association constant is diffusion-related. On the other hand, the measured value of k_{off} decreases with the temperature and is always smaller

than for inert eGFP (where we found $k_{off} = 240.5$ s^{-1}). Therefore, k_{off} partially accounts for more specific heat-shock-activated interactions.

Specific binding sites are heterogeneously distributed

To confirm our hypothesis according to which HSF1 diffusion constant after heat shock reflects specific interactions with DNA binding sites, we investigated the spatial variations of the measured parameters of the reaction-dominant model. Previous studies have shown that the heat-shock response correlates with an increase in the number of specific DNA binding sites for HSF1, but this number is still limited. We thus expect to observe a more pronounced intracellular variability at 43°C. Therefore, we calculated, for each cell, the variation coefficients of D, $k_{on}*$, and k_{off}, defined as the ratio of the SD to the mean value of the measurements provided by different spots within the cell. Although the variation coefficients of $k_{on}*$ and k_{off} (0.90 and 0.57, respectively) do not vary after heat shock, that of the diffusion constant, D, goes from 0.63 at 37°C, to 1.02 at 43°C (*t*-test gives $p < 10^{-5}$). This can be attributed to the specific part of the interactions of HSF1 with DNA, activated by heat shock, that would cause the effective diffusion constant to decrease. Because these specific interactions are localized on a limited number of sites, they induce a higher spatial inhomogeneity (evaluated with the variation coefficient) of the measured diffusion constant. To confirm this interpretation, we have also calculated the variation coefficient of the diffusion constant of inert eGFP molecules and found the same value, 0.4, before and after heat shock. This indicates that the chromatin structure, which is modified by heat shock, does not impact on diffusion inhomogeneity.

DISCUSSION

The diffusion of eGFP has been recently shown to be slower within dense heterochromatic deacetylated regions of the genome than within acetylated euchromatic regions (39). Since deacetylation of histones occurs upon heat shock (29), the corresponding modifications of chromatin structure should induce a lower mobility. Conversely, in solution, the diffusion constant increases with temperature, mainly because of the viscosity dependence (see Fig. S7). Since the mobility of eGFP in living cells does not significantly vary upon stress (Fig. 1 *B*), opposite impacts of chromatin deacetylation and viscosity effect probably compensate each other in living cells and thus can be laid aside in the forthcoming discussion.

HSF1 activation is a multistep complex process involving multiple partners. In non-heat-shocked cells, HSF1 is present as monomers bound to several proteins including HSP70, HSP90, and histone deacetylase 6 (HDAC6) (40). In heat-shocked cells, HSF1 dissociates from its chaperones, trimerizes, and is found to interact with histone acetyl

transferases (HATs) and HDAC1 and HDAC2 (29). Like other transcription factors (41), HSF1 diffusion is delayed by interactions with DNA, so that the diffusion constant is most likely effective. In addition, our measured k_{off} constants are intermediate between specific (0.1 s^{-1}) and aspecific transient binding (325 s^{-1}) values found in the case of Hox transcription factor (42). Our mFCS experiments most likely reveal the coexistence of low- and high-affinity HSF1 binding sites. The first would correspond to weak HSF1-DNA binding interactions resulting from multiple association/dissociation events occurring in the search of HSF1 for specific HSE target sites (43). The second corresponds to HSF1 specific binding to DNA targets after heat shock.

The heterogeneity that we found in stressed cells could result from the low number of specific HSF1-DNA binding sequences: 768 HSE sites have been identified in human cells from a database of >10,000 putative promoters, only half of which bound to HSF1 in heat-shocked cells (44). Additional HSE elements have been identified in the vicinity of a number of Alu sequences present in an inverse orientation with regard to transcriptionally repressed genes upon heat shock (45). The existence of a low number of HSF1 DNA targets with a genome-wide distribution would explain the diffusion-constant heterogeneity we have observed.

In Hela cells, the HSF1 dynamics is similar to that already reported for other transcription factors: nuclear steroid receptors (46–50), the tumor suppressor gene p53 (51), the TATA binding protein (TBP), and TBP-associated factors (TAFs) (52) studied by FRAP in the nucleoplasm. However, this contrasts with the particularly slow HSF1 dynamics previously reported in *Drosophila* (53). It is worthwhile to note that this latter study was performed only on specific HSF1-DNA-binding chromosomal sites and not in the nucleoplasm. As stressed by McNally and co-authors (47–50,54), however, caution should be taken when comparing data from the literature, in particular when comparing different acquisition techniques (FRAP, FCS, SMT) and modeling methods. A recent publication was specifically devoted to the cross-validation of FCS and FRAP, and it stressed the need to quantify the impact of photobleaching on in vivo binding estimates (49). We therefore believe that it would be interesting to combine mFCS and FRAP-like approaches, which should permit the study of molecular interactions at short and long timescales in combination with HSF1 mutated in its DNA binding domain.

CONCLUSIONS

We have shown that our mFCS setup makes it possible to study changes of HSF1 dynamics in heat-shocked cells. Whereas a standard FCS apparatus would have required sequentially moving the laser spot to the positions of interest within the cells, we could simultaneously (i.e., in parallel) acquire the corresponding autocorrelation functions, thus saving a considerable amount of time. This is crucial when studying a transient phenomenon such as the cellular response to heat. Not only does it save time, but it also improves the quality of the statistical data and permits further analysis, such as the study of intracellular variability of the dynamic parameters (diffusion and reaction constants). Although the use of five measurement volumes in parallel comes at the price of lower time resolution compared to standard FCS, the 14 μs temporal resolution is amply sufficient for the phenomena we observed (shorter diffusion times were of the order of 200 μs). Therefore, to date we do not see any disadvantage of the mFCS technique, except the relative complexity needed to run it.

Concerning our study of heat shock, the mFCS experiments put into evidence weakly specific interactions of HSF1 with DNA sites homogeneously distributed within the nucleus, superimposed on more specific and much less numerous (i.e., more heterogeneous) interaction sites. Fluorescence cross-correlation spectroscopy or two-color, two-dimensional fluorescence intensity distribution analysis would be complementary approaches (55), as they should provide information about trimerization of HSF1 after heat shock, or interactions with identified partners, such as chaperones. The observed intranuclear variability of diffusion also suggests that in future experiments, it will be important to combine the detection of HSF1 with markers of euchromatin and heterochromatin. However, fluorescence cross talk should be carefully prevented. Finally, it would no doubt be interesting to combine FCS and FRAP-like approaches, as has been done to study the dynamics of the heterochromatin factor HP1 (56), since it should permit analysis of HSF1 interactions at short and long timescales. This will be the future focus of our work on the heat-shock response.

SUPPORTING MATERIAL

REFERENCES

1. Petersen, N. O., P. L. Höddelius, …, K. E. Magnusson. 1993. Quantitation of membrane receptor distributions by image correlation spectroscopy: concept and application. *Biophys. J.* 65:1135–1146.

2. Wiseman, P. W., and N. O. Petersen. 1999. Image correlation spectroscopy. II. Optimization for ultrasensitive detection of preexisting platelet-derived growth factor-β receptor oligomers on intact cells. *Biophys. J.* 76:963–977.

3. Wiseman, P. W., C. M. Brown, ..., A. F. Horwitz. 2004. Spatial mapping of integrin interactions and dynamics during cell migration by image correlation microscopy. *J. Cell Sci.* 117:5521–5534.

4. Digman, M. A., P. W. Wiseman, ..., E. Gratton. 2009. Detecting protein complexes in living cells from laser scanning confocal image sequences by the cross correlation raster image spectroscopy method. *Biophys. J.* 96:707–716.

5. Gielen, E., N. Smisdom, ..., M. Ameloot. 2009. Measuring diffusion of lipid-like probes in artificial and natural membranes by raster image correlation spectroscopy (RICS): use of a commercial laser-scanning microscope with analog detection. *Langmuir.* 25:5209–5218.

6. Digman, M. A., C. M. Brown, ..., E. Gratton. 2005. Measuring fast dynamics in solutions and cells with a laser scanning microscope. *Biophys. J.* 89:1317–1327.

7. Grüner, N., J. Capoulade, ..., M. Wachsmuth. 2010. Measuring and imaging diffusion with multiple scan speed image correlation spectroscopy. *Opt. Express.* 18:21225–21237.

8. Kannan, B., L. Guo, ..., T. Wohland. 2007. Spatially resolved total internal reflection fluorescence correlation microscopy using an electron multiplying charge-coupled device camera. *Anal. Chem.* 79:4463–4470.

9. Capoulade, J., M. Wachsmuth, ..., M. Knop. 2011. Quantitative fluorescence imaging of protein diffusion and interaction in living cells. *Nat. Biotechnol.* 29:835–839.

10. Ruan, Q., M. A. Cheng, ..., W. W. Mantulin. 2004. Spatial-temporal studies of membrane dynamics: scanning fluorescence correlation spectroscopy (SFCS). *Biophys. J.* 87:1260–1267.

11. Amediek, A., E. Haustein, ..., P. Schwille. 2002. Scanning dual-color cross-correlation analysis for dynamic co-localization studies of immobile molecules. *Single Molecules.* 4:201–210.

12. Skinner, J. P., Y. Chen, and J. D. Müller. 2005. Position-sensitive scanning fluorescence correlation spectroscopy. *Biophys. J.* 89:1288–1301.

13. Ries, J., and P. Schwille. 2006. Studying slow membrane dynamics with continuous wave scanning fluorescence correlation spectroscopy. *Biophys. J.* 91:1915–1924.

14. Pan, X., H. Yu, ..., T. Wohland. 2007. Characterization of flow direction in microchannels and zebrafish blood vessels by scanning fluorescence correlation spectroscopy. *J. Biomed. Opt.* 12: 014034, 014034–10.

15. Ries, J., S. R. Yu, ..., P. Schwille. 2009. Modular scanning FCS quantifies receptor-ligand interactions in living multicellular organisms. *Nat. Methods.* 6:643–645.

16. Digman, M. A., and E. Gratton. 2009. Imaging barriers to diffusion by pair correlation functions. *Biophys. J.* 97:665–673.

17. Petrásek, Z., S. Derenko, and P. Schwille. 2011. Circular scanning fluorescence correlation spectroscopy on membranes. *Opt. Express.* 19:25006–25021.

18. Ferrand, P., M. Pianta, ..., D. Marguet. 2009. A versatile dual spot laser scanning confocal microscopy system for advanced fluorescence correlation spectroscopy analysis in living cell. *Rev. Sci. Instrum.* 80:083702.

19. Sisan, D. R., R. Arevalo, ..., J. S. Urbach. 2006. Spatially resolved fluorescence correlation spectroscopy using a spinning disk confocal microscope. *Biophys. J.* 91:4241–4252.

20. Needleman, D. J., Y. Xu, and T. J. Mitchison. 2009. Pin-hole array correlation imaging: highly parallel fluorescence correlation spectroscopy. *Biophys. J.* 96:5050–5059.

21. Oh, D., A. Zidovska, ..., D. J. Needleman. 2011. Development of time-integrated multipoint moment analysis for spatially resolved fluctuation spectroscopy with high time resolution. *Biophys. J.* 101: 1546–1554.

22. Curtis, J. E., B. A. Koss, and D. G. Grier. 2002. Dynamic holographic optical tweezers. *Opt. Commun.* 207:169–175.

23. Blancquaert, Y., J. Gao, ..., A. Delon. 2008. Spatial fluorescence cross-correlation spectroscopy by means of a spatial light modulator. *J. Biophotonics.* 1:408–418.

24. Burkhardt, M., and P. Schwille. 2006. Electron multiplying CCD based detection for spatially resolved fluorescence correlation spectroscopy. *Opt. Express.* 14:5013–5020.

25. Kannan, B., J. Y. Har, ..., T. Wohland. 2006. Electron multiplying charge-coupled device camera based fluorescence correlation spectroscopy. *Anal. Chem.* 78:3444–3451.

26. Matsumoto, M., T. Sugiura, and K. Minato. 2007. Spatially resolved fluorescence correlation spectroscopy based on electron multiplying CCD. *Proc. SPIE, Munich.* 6630:663017.

27. Tyndall, D., R. Walker, ..., R. Henderson. 2011. Automatic laser alignment for multifocal microscopy using a LCOS SLM and a 32×32 pixel CMOS SPAD array. Proc. SPIE 8086.

28. Galland, R., J. Gao, ..., A. Delon. 2011. Multi-confocal fluorescence correlation spectroscopy: experimental demonstration and potential applications for living cell measurements. *Front. Biosci.* 3:476–488.

29. Fritah, S., E. Col, ..., C. Vourc'h. 2009. Heat-shock factor 1 controls genome-wide acetylation in heat-shocked cells. *Mol. Biol. Cell.* 20:4976–4984.

30. Jolly, C., A. Metz, ..., C. Vourc'h. 2004. Stress-induced transcription of satellite III repeats. *J. Cell Biol.* 164:25–33.

31. Akerfelt, M., R. I. Morimoto, and L. Sistonen. 2010. Heat shock factors: integrators of cell stress, development and lifespan. *Nat. Rev. Mol. Cell Biol.* 11:545–555.

32. Cojoc, D., E. Di Fabrizio, ..., S. Cabrini. 2003. Spherical-based approach to design diffractive optical elements. *Proc. SPIE.* 5227:123–131.

33. Michelman-Ribeiro, A., D. Mazza, ..., J. G. McNally. 2009. Direct measurement of association and dissociation rates of DNA binding in live cells by fluorescence correlation spectroscopy. *Biophys. J.* 97:337–346.

34. Donnert, G., C. Eggeling, and S. W. Hell. 2007. Major signal increase in fluorescence microscopy through dark-state relaxation. *Nat. Methods.* 4:81–86.

35. Petrásek, Z., and P. Schwille. 2008. Precise measurement of diffusion coefficients using scanning fluorescence correlation spectroscopy. *Biophys. J.* 94:1437–1448.

36. Dross, N., C. Spriet, ..., J. Langowski. 2009. Mapping eGFP oligomer mobility in living cell nuclei. *PLoS ONE.* 4:e5041.

37. Baler, R., G. Dahl, and R. Voellmy. 1993. Activation of human heat shock genes is accompanied by oligomerization, modification, and rapid translocation of heat shock transcription factor HSF1. *Mol. Cell. Biol.* 13:2486–2496.

38. Sarge, K. D., S. P. Murphy, and R. I. Morimoto. 1993. Activation of heat shock gene transcription by heat shock factor 1 involves oligomerization, acquisition of DNA-binding activity, and nuclear localization and can occur in the absence of stress. *Mol. Cell. Biol.* 13:1392–1407.

39. Bancaud, A., S. Huet, ..., J. Ellenberg. 2009. Molecular crowding affects diffusion and binding of nuclear proteins in heterochromatin and reveals the fractal organization of chromatin. *EMBO J.* 28:3785–3798.

40. Boyault, C., Y. Zhang, ..., S. Khochbin. 2007. HDAC6 controls major cell response pathways to cytotoxic accumulation of protein aggregates. *Genes Dev.* 21:2172–2181.

41. Karpova, T. S., T. Y. Chen, ..., J. G. McNally. 2004. Dynamic interactions of a transcription factor with DNA are accelerated by a chromatin remodeller. *EMBO Rep.* 5:1064–1070.

42. Vukojevic, V., D. K. Papadopoulos, ..., R. Rigler. 2010. Quantitative study of synthetic Hox transcription factor-DNA interactions in live cells. *Proc. Natl. Acad. Sci. USA.* 107:4093–4098.

43. Hager, G. L., J. G. McNally, and T. Misteli. 2009. Transcription dynamics. *Mol. Cell.* 35:741–753.

44. Trinklein, N. D., J. I. Murray, ..., R. M. Myers. 2004. The role of heat shock transcription factor 1 in the genome-wide regulation of the mammalian heat shock response. *Mol. Biol. Cell.* 15:1254–1261.

45. Pandey, R., A. K. Mandal, …, M. Mukerji. 2011. Heat shock factor binding in Alu repeats expands its involvement in stress through an antisense mechanism. *Genome Biol.* 12:R117.

46. Darzacq, X., J. Yao, …, R. H. Singer. 2009. Imaging transcription in living cells. *Annu Rev Biophys.* 38:173–196.

47. Mueller, F., P. Wach, and J. G. McNally. 2008. Evidence for a common mode of transcription factor interaction with chromatin as revealed by improved quantitative fluorescence recovery after photobleaching. *Biophys. J.* 94:3323–3339.

48. Stasevich, T. J., F. Mueller, …, J. G. McNally. 2010. Dissecting the binding mechanism of the linker histone in live cells: an integrated FRAP analysis. *EMBO J.* 29:1225–1234.

49. Stasevich, T. J., F. Mueller, …, J. G. McNally. 2010. Cross-validating FRAP and FCS to quantify the impact of photobleaching on in vivo binding estimates. *Biophys. J.* 99:3093–3101.

50. Stasevich, T. J., and J. G. McNally. 2011. Assembly of the transcription machinery: ordered and stable, random and dynamic, or both? *Chromosoma.* 120:533–545.

51. Hinow, P., C. E. Rogers, …, E. DiBenedetto. 2006. The DNA binding activity of p53 displays reaction-diffusion kinetics. *Biophys. J.* 91: 330–342.

52. de Graaf, P., F. Mousson, …, H. T. Timmers. 2010. Chromatin interaction of TATA-binding protein is dynamically regulated in human cells. *J. Cell Sci.* 123:2663–2671.

53. Yao, J., K. M. Munson, …, J. T. Lis. 2006. Dynamics of heat shock factor association with native gene loci in living cells. *Nature.* 442:1050–1053.

54. Mueller, F., D. Mazza, …, J. G. McNally. 2010. FRAP and kinetic modeling in the analysis of nuclear protein dynamics: what do we really know? *Curr. Opin. Cell Biol.* 22:403–411.

55. Elson, E. L. 2011. Fluorescence correlation spectroscopy: past, present, future. *Biophys. J.* 101:2855–2870.

56. Müller, K. P., F. Erdel, …, K. Rippe. 2009. Multiscale analysis of dynamics and interactions of heterochromatin protein 1 by fluorescence fluctuation microscopy. *Biophys. J.* 97:2876–2885.

57. Müller, C. B., A. Loman, …, J. Enderlein. 2008. Precise measurement of diffusion by multi-color dual-focus fluorescence correlation spectroscopy. *Europhys. Lett.* 83:46001.